Available online at www.sciencedirect.com
ScienceDirect
Trans. Nonferrous Met. Soc. China 32(2022) 483−492
Transactions of Nonferrous Metals Society of China
www.tnmsc.cn

Fine-grained Mg−1Mn−0.5Al−0.5Ca−0.5Zn alloy with high strength and good ductility fabricated by conventional extrusion

Guang-lin GU[1,2], Xiang-nan KE[1], Fa-ping HU[1], Shu-jie ZHAO[1], Guo-bin WEI[1], Yan YANG[1], Xiao-dong PENG[1], Wei-dong XIE[1]

1. Joint International Laboratory for Light Alloys, College of Materials Science and Engineering, Chongqing University, Chongqing 400044, China;
2. Guizhou Anda Aviation Forging Co., Ltd., Anshun 561005, China

Received 9 January 2021; accepted 30 August 2021

Abstract: Mg−1Mn−0.5Al−0.5Ca−0.5Zn (wt.%) alloy was fabricated by conventional extrusion at 673 K with an extrusion ratio of 25:1, followed by aging at 473 K. The microstructure was characterized by scanning electron microscopy, electron back-scattered diffraction, and transmission electron microscopy. The mechanical properties were determined by the tensile test. The peak-aged sample shows fine recrystallized grains with an average grain size of 1.7 μm. Area fraction of Al−Ca particles in the alloy increases significantly after peak aging. Meanwhile, both ⟨*a*⟩ and ⟨*c*+*a*⟩ dislocations were observed to remain in the alloy after hot extrusion. Thus, the peak-aged sample exhibits simultaneously high strength and good ductility with the ultimate tensile stress, tensile yield stress, and tension fracture elongation of 320 MPa, 314 MPa, and 19.0%, respectively.

Key words: Mg−Mn−Al−Ca−Zn alloy; fine grain; precipitate; strength; ductility

1 Introduction

Mg alloys are promising lightweight structural materials used in the automotive, aircraft, aerospace, and 3C industries, owing to the merits of low density, high specific strength, good casting ability, high damping capacity, and so on [1,2]. However, several challenges, such as low strength and poor ductility at the ambient temperature, are urgent to overcome for the broad applications of Mg alloys [3,4].

The poor room-temperature formability of magnesium alloys is due to the inherent closed-packed hexagonal (hcp) structure of magnesium alloys with a *c*/*a* ratio of 1.624, and the lack of sufficient independent slip systems to fulfill the requirement of uniform deformation (von Mises criterion). The low critical resolved shear stress (CRSS) of basal ⟨*a*⟩ slip and tension twinning is also responsible for the low strength of the alloys. By contrast, ⟨*c*+*a*⟩ dislocation can provide five independent slip systems. Its cross-slip and interaction with other deformation mechanisms are favorable for improving strength and ductility [5]. Therefore, research aimed to explore the mechanism of ⟨*c*+*a*⟩ slip and to promote the activation of ⟨*c*+*a*⟩ slip has been extensively carried out [6−8]. Whereas, twinning, especially tension twinning, is much more common than ⟨*c*+*a*⟩ slip in Mg alloys due to the very high CRSS of ⟨*c*+*a*⟩ slip. Recently, a transition of deformation mechanism has been observed both in pure Mg [9] and Mg alloy [10]. When the grain size is smaller than a critical size leading to the ⟨*c*+*a*⟩ and ⟨*a*⟩ slips-dominating deformation, twinning is inhibited.

Corresponding author: Wei-dong XIE, Tel: +86-13508306908, E-mail: wdxie@cqu.edu.cn;
Guang-lin GU, Tel: +86-17318486324, E-mail: 2749583306@qq.com
DOI: 10.1016/S1003-6326(22)65809-6

Excellent ductility and high strength are achieved, accompanied by the slip-dominating deformation.

Alloys produced by severe plastic deformation usually exhibit limited ductility due to remained high density of dislocations and grain boundaries in the alloys. Hot extrusion is a suitable way to solve this problem. With proper process parameters and alloy components, the results show that defects can be significantly decreased during deformation and fine-grained microstructure could be obtained. On this basis, a series of fine-grained Mg alloys have been designed and fabricated by low-temperature extrusion [11−13], exhibiting an excellent combination of strength and ductility. Deformation should be carried out at low temperature and high extrusion ratio to accumulate strain as much as possible to refine grain size. Thus, these extruded Mg alloys are added with some elements, such as Mn, to improve their extrudability [11]. The addition of Mn element can form nano α-Mn precipitates in the Mg alloy, significantly refining the grain size [14]. The co-addition of Mn and Al will result in Al_8Mn_5 precipitates providing a dispersion strengthening [11]. Otherwise, the high elongations of about 30% and 50% were achieved by Mg−0.4Al alloying with various Mn [11]. To further enhance the strength of the alloy, a small amount of Ca and Zn were added into the Mg−Al−Mn alloy to refine the grain size and promote the formation of GP zone (Al_2Ca) during the artificially aging treatment [3,14−16].

In this work, an age hardening Mg−1Mn−0.5Al−0.5Ca−0.5Zn (wt.%) alloy was fabricated by conventional extrusion at 673 K with an extrusion ratio of 25:1. After aging treatment at 473 K for 1 h, the alloy exhibits excellent comprehensive mechanical properties with a tensile yield stress of 314 MPa and a tension fracture elongation of 19%. The developed alloy is expected to have a broad application prospect in the automotive industry.

2 Experimental

Mg−1Mn−0.5Al−0.5Ca−0.5Zn (wt.%) alloy was produced by high purity Mg (99.9%), Al (99.8%), Zn (99.9%), Mg−20Ca, and Mg−3Mn master alloys in a *d*89 mm cylindrical steel crucible, under the protection of mixture gas of CO_2 and SF_6 (volume ratio of 100:1) at 993.5 K, followed by water chilling to about 373 K within 2 min. The casting ingots were homogenized at 623 K for 8 h and then machined into *d*80 mm billets. Next, the billets were preheated at 673 K for 30 min, followed by hot extrusion into *d*16 mm bars at 673 K and air cooling subsequently.

The cuboid samples with sizes of 10 mm × 10 mm × 8 mm and dog-bone-shaped samples with a gauge length of 12.5 mm were machined from the center of the extruded bars along the extrusion direction (ED) for hardness and tensile tests. Aging treatment was conducted at 473 K after hot extrusion with different time, i.e., 20 min, 40 min, 1 h, 2 h, 4 h, 8 h, 16 h, and 24 h. The hardness tests were carried out on a micro-hardness tester (HVS−50T). Tensile tests were carried out on a SANS CMT−5015 tension machine with a consistent strain rate of 0.5 mm/min. For simplicity, the samples were dubbed as T_{ex}, $T_{0.33}$, T_1, and T_8 for as-extruded, 20 min, 1, and 8 h aging-treated alloy, respectively.

Microstructure and texture were characterized by a scanning electron microscope (SEM, JEOL JSM−7800F) equipped with an Oxford Aztec EBSD, energy dispersive spectrometer (EDS) detector, and transmission electron microscope (TEM, JEM−2100). The samples for SEM and EDS observation were mechanically ground and then etched with a solution of picric acid (4 g), acetic acid (20 mL), ethanol (60 mL), and water (20 mL). Samples for EBSD mapping were prepared by mechanical grinding followed by electro-polishing at around 253 K for 2 min with the solution mixed with 5 vol.% perchloric acid and 95 vol.% alcohol. The EBSD mapping was acquired at 20 kV with a step size of 0.2 μm. TEM samples were prepared by ion milling, and observed under 200 kV accelerating voltage. The grain size, precipitate size, and the fraction of precipitates were measured using the Image-Pro.

3 Results and discussion

3.1 Microstructure

Figure 1 shows the grain structure and the grain size distribution of T_{ex} and T_1. Both samples exhibited equiaxed dynamically recrystallized (DRXed) grains which are uniformly distributed. A few low angle boundaries (the white curves in Figs. 1(a) and (c)) are readily observed in some grains. The average grain sizes of T_{ex} and T_1 are 1.8

and 1.7 μm, respectively. The difference in the microstructure between T_{ex} and T_1 is negligible, attributing to the low artificial aging temperature.

Figure 2 presents the pole figures (PFs) of T_{ex} and T_1. Both T_{ex} and T_1 exhibit a strong texture with basal planes of most grains approximately parallel to extrusion direction (ED), and the maximum intensities are 17.7 and 14.9, respectively. This type of texture has also been detected in other fully recrystallized Mg alloys after hot extrusion [11,17]. Except for the slight difference in texture intensity, the PFs of T_{ex} and T_1 are quite similar, which is consistent with Fig. 1.

The Schmid factor (SF) of the main deformation modes were calculated based on the EBSD mapping, as shown in Fig. 3. Due to the strong texture of the investigated alloy, the SF of basal $\langle a \rangle$ slips for most grains is very low while those of nonbasal $\langle a \rangle$ and $\langle c+a \rangle$ slip are comparatively high, leading to the most grains deformed by activating the nonbasal $\langle a \rangle$ and $\langle c+a \rangle$ slip, as shown in Fig. 3(a).

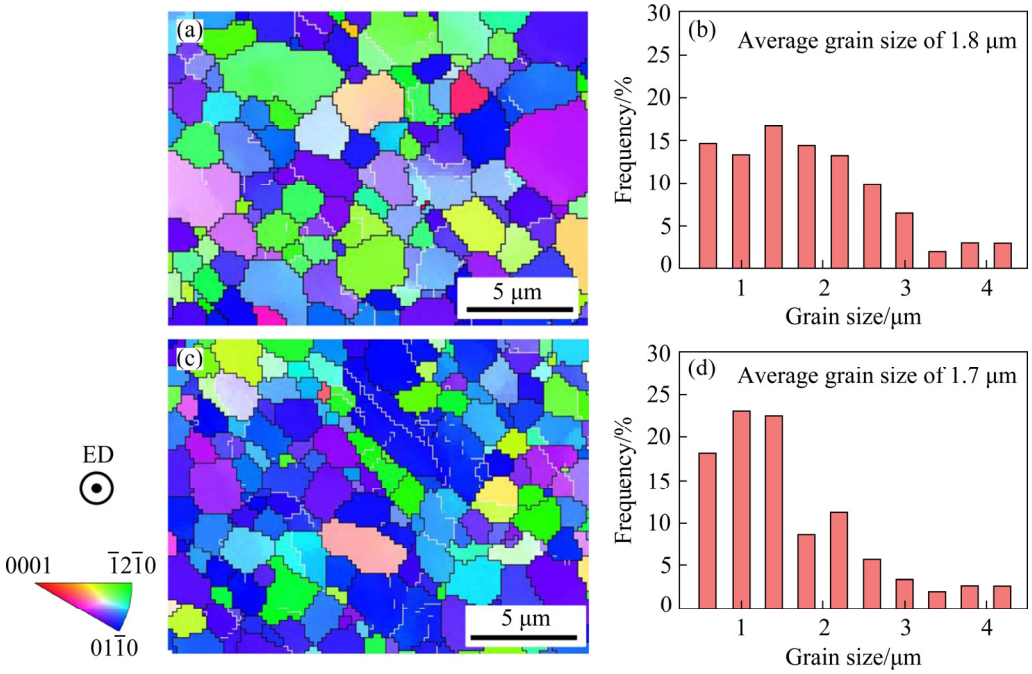

Fig. 1 EBSD IPF maps (a, c) and grain size distributions (b, d) of Mg−1Mn−0.5Al−0.5Ca−0.5Zn alloy: (a, b) T_{ex}; (c, d) T_1

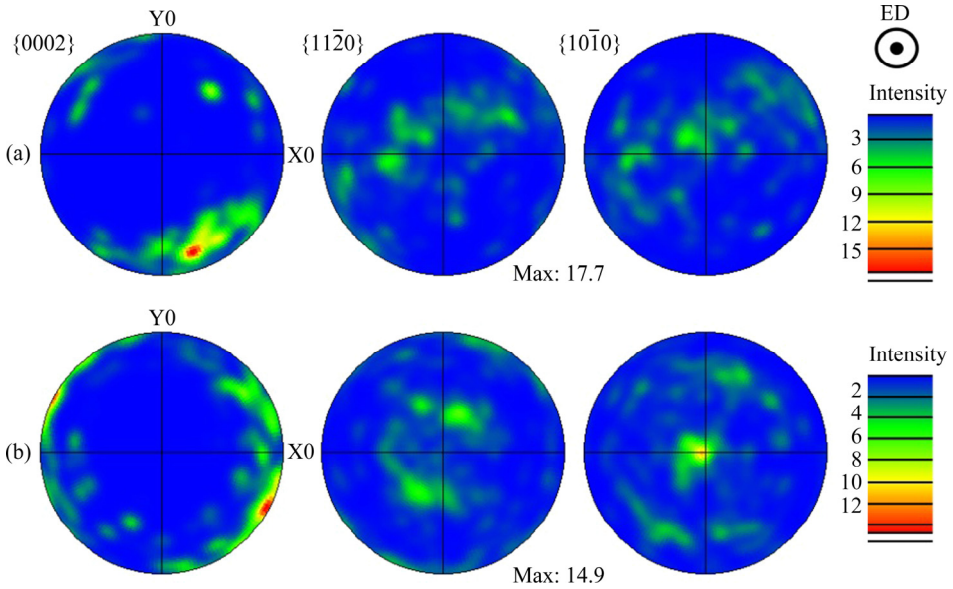

Fig. 2 PFs of Mg−1Mn−0.5Al−0.5Ca−0.5Zn alloy taken from plane perpendicular to ED of samples, showing texture structure of as-extruded condition (a) and aged at 473 K for 1 h (b)

Figure 3(b) shows that the frequencies of grains with SF higher than 0.4 are 80.0% and 56.0% for nonbasal ⟨*a*⟩ and ⟨*c*+*a*⟩ slip, respectively, while that is 5.8% for basal ⟨*a*⟩ slip. It should be noted that extension twinning usually plays an important role in the deformation of coarse-grained Mg alloys. However, the fine grains of the investigated alloys will significantly restrict the activation of extension twinning [11]. LUO et al [18] illustrated that extension twins are totally eliminated when the grain sizes are smaller than 5 μm in Mg−3Gd. Moreover, the activation of nonbasal slips will cause a strong cross slip between basal and nonbasal slips, which is favorable to improving the strength and ductility of the alloy [11].

Figure 4 shows the morphology of the precipitates of T_{ex} and T_1, where the intermetallic-compounds particles marked by red arrows were analyzed by EDS (see Table 1). The particles are uniformly distributed in the images taken from ED (Figs. 4(a) and (b)), while the particles are

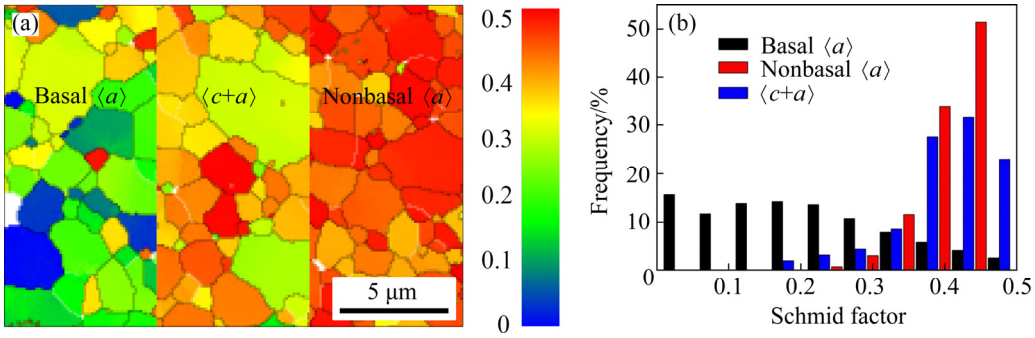

Fig. 3 SF of different deformation modes in Mg−1Mn−0.5Al−0.5Ca−0.5Zn alloy under hot extrusion: (a) SF coloring maps; (b) SF distribution frequency of each deformation mode

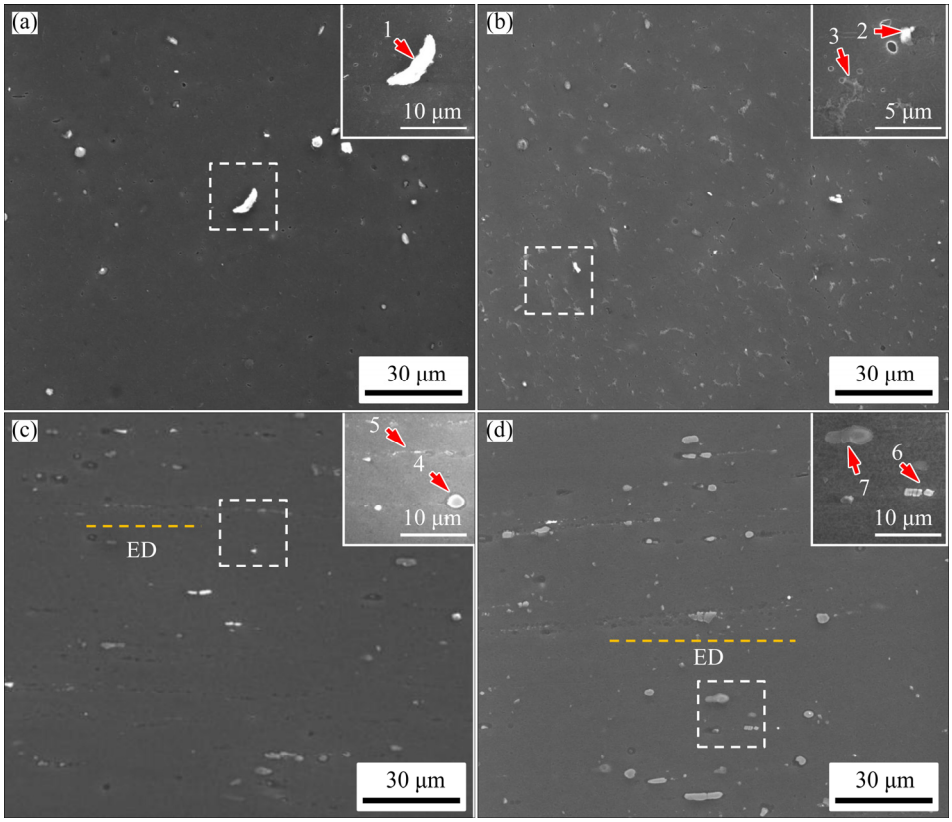

Fig. 4 SEM images taken from ED of samples T_{ex} (a) and T_1 (b) and taken from direction perpendicular to ED of T_{ex} (c) and T_1 (d) (The insets in the top right-hand corner of each micrograph are enlarged micrographs corresponding to boxed areas by dash lines in each image, where the numbered 7 intermetallic compounds were analyzed by EDS (The inserted dash yellow lines are ED)

Table 1 EDS elemental analysis results of intermetallic-compounds particles marked by red arrows in Fig. 4 (at.%)

Position No.	Mg	Mn	Al	Ca	Zn	Phase
1	38.6	30.3	30.9	0.0	0.1	Al−Mn
2	53.2	20.5	25.8	0.3	0.2	Al−Mn
3	79.8	0.1	8.1	11.4	0.5	Al−Ca
4	65.1	19.0	15.4	0.2	0.4	Al−Mn
5	77.2	0.3	9.2	12.7	0.6	Al−Ca
6	61.1	17.7	20.9	0.1	0.2	Al−Mn
7	85.5	0.4	6.8	6.8	0.5	Al−Ca

necklace-shaped and distributed along with ED in the images taken from the direction perpendicular to ED (Figs. 4(c) and (d)). There are two kinds of particles, the brighter ones (particles 1, 2, 4, and 6) and the darker ones (particles 3, 5, and 7). The EDS results demonstrate that the brighter particles should be Al−Mn phase, while the darker particles should be Al−Ca phase, which are consistent with previous research [19]. The average diameters of Al−Mn particles are measured as 2.8 and 2.1 μm in the T_{ex} and T_1 samples, respectively. And the average diameters of Al−Ca particles are 1.9 and 2.4 μm in the T_{ex} and T_1 samples, respectively.

It can be found from Fig. 5 that a significant increase in quantity occurs in precipitates after aging treatments, especially the area fraction of the Al−Ca phase that is obviously increased from 0.9% to 6.3%. Also, it is noted that the EDS results presented in Table 1, show that Al−Mn phases are detected in most samples. Nevertheless, only 0.3% Al−Mn particles were observed in the T_1 samples,

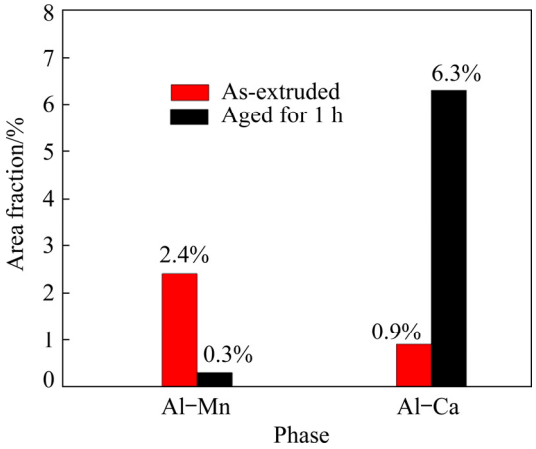

Fig. 5 Area fraction of Al−Mn and Al−Ca phases in T_{ex} and T_1 samples, taken from SEM images shown in Fig. 4

which is attributed to the formation of more Al−Ca precipitates after aging treatment that consumes more Al. In addition, the $Mg_{17}Al_{12}$ phase was rarely detected, indicating that it may dissolve into the matrix during the hot extrusion.

It has been widely reported that alloying with Mn can result in nano-sized α-Mn precipitates in Mg−Mn-based alloys, and it will form Al_8Mn_5 precipitates when Al and Mn are added to the alloy in the meantime [15]. The nano-sized precipitates morphology can be observed in Fig. 6(b). The formation of these precipitates will significantly refine the dynamically recrystallized (DRXed) grains of the investigated Mg alloy during hot extrusion. In addition, the precipitates can hinder the growth of recrystallization grain and promote the recrystallization nucleation [15,20]. What's more, the growth of abnormal recrystallization grain is also dramatically restricted by the precipitates [21].

The TEM bright-field images of the equiaxed recrystallized grains and a high density of nano-sized precipitates are illustrated in Figs. 6(a) and (b), respectively. $\langle a \rangle$ dislocations and $\langle c+a \rangle$ dislocations can be clearly observed in Fig. 7. The grains are equiaxed (Fig. 6(a)), owing to the fully dynamic recrystallization, and a high density of dislocations accumulate inside the deformed grain (Fig. 6(a)). And some fine precipitates about 20 nm in diameter are formed in the matrix (Fig. 6(b)), which benefits the improvement of strength and ductility. According to the Orowan equation, $\tau=(GB)/\lambda$, where T is the critical shear stress for the glide dislocations, G is the matrix shear modulus, B is the Burgers vector, and λ is the particle spacing. When the volume fraction of particles remains unchanged, the finer the particles are, the smaller the particle spacing is, and the greater the critical shear stress is. The critical shear stress (τ) for the glide dislocations to pass through barriers of hard particles is inversely related to the particle size. Therefore, the observed nano-sized precipitates in Mg−1Mn−0.5Al−0.5Ca−0.5Zn results in larger T and therefore high yield strength.

The main deformation mechanisms for the hot-extrusion deformation of the investigated alloy were characterized with two-beam bright-field images and dark-field images to reveal the origin of good ductility in the as-extruded samples, as shown in Fig. 7. Two types of $\langle a \rangle$ and $\langle c+a \rangle$ dislocations

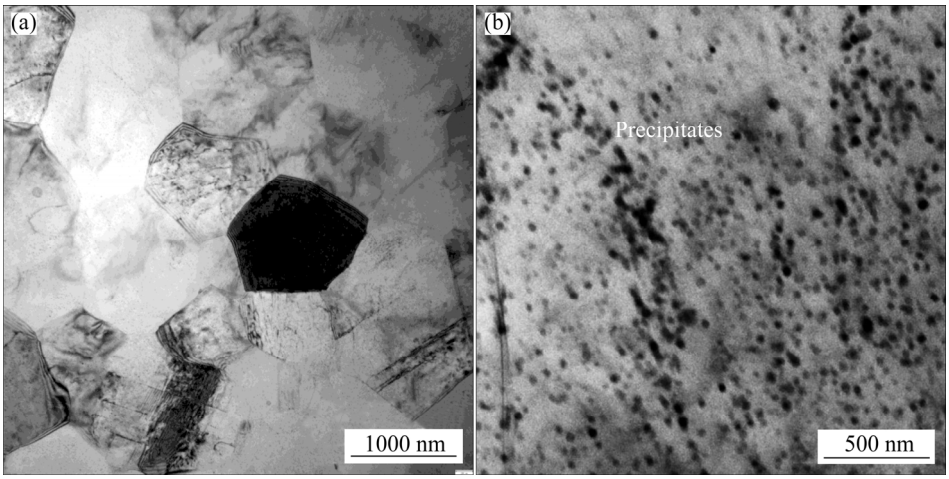

Fig. 6 TEM images of as-extruded Mg−1Mn−0.5Al−0.5Ca−0.5Zn alloy in condition of grain topography of T_{ex} (a) and precipitate morphology (b)

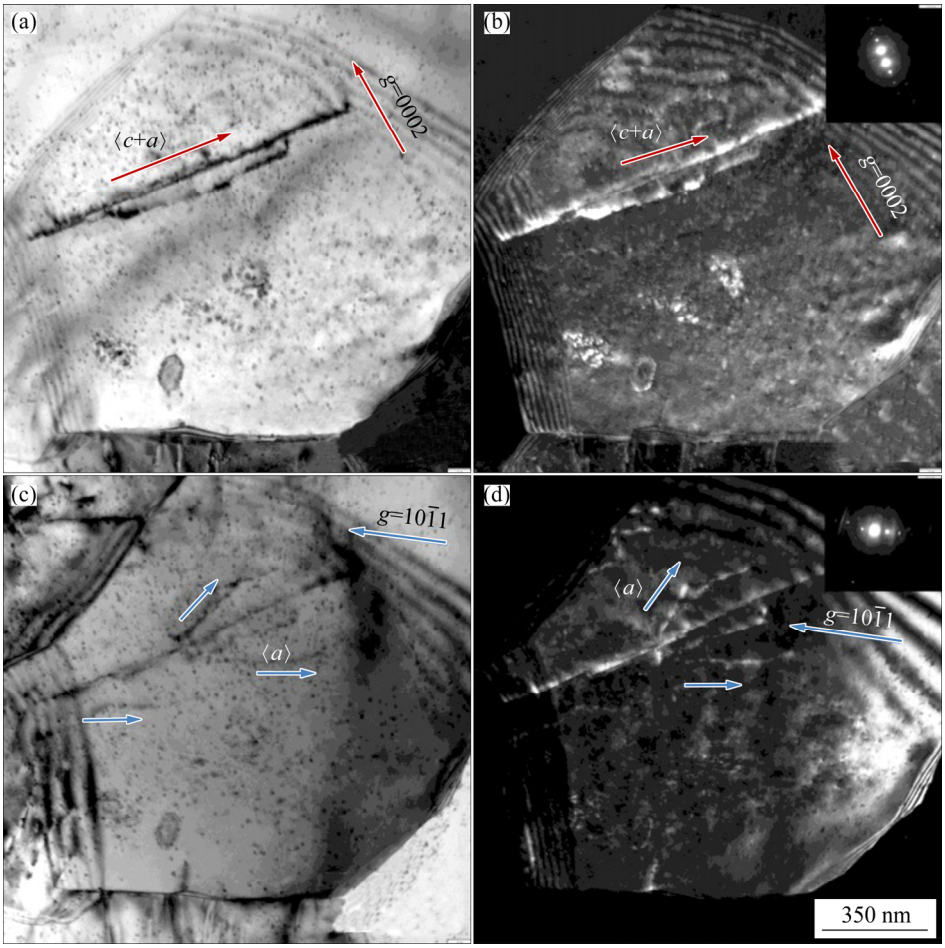

Fig. 7 TEM images showing dislocation morphology in as-extruded Mg−1Mn−0.5Al−0.5Ca−0.5Zn alloy: (a, b) TEM bright-field and dark-field images of ⟨*c*+*a*⟩ dislocations under *g*=0002, respectively; (c, d) TEM bright-field and dark-field images of ⟨*a*⟩ dislocations under $g=10\bar{1}1$, respectively

dominate in the as-extruded samples with a grain size of 1.8 μm. ⟨*c*+*a*⟩ dislocations can be clearly detected under *g*=0002, indicated by red arrows in Figs. 7(a) and (b), which generate ⟨*c*+*a*⟩ slips during the hot-extrusion deformation. A few ⟨*a*⟩ dislocations were observed under $g=10\bar{1}1$, indicated by blue arrows shown in Figs. 7(c) and (d). It is owing to that the SF value of ⟨*c*+*a*⟩ and nonbasal ⟨*a*⟩ slip

systems in most grains is close to 0.45, as shown in Fig. 3. No twins are found in the as-extruded samples due to the fine grains with an average grain size of 1.8 μm. ⟨*c*+*a*⟩ slip and nonbasal ⟨*a*⟩ slip can be activated during the hot-extrusion deformation, instead of twinning and basal ⟨*a*⟩ slip which dominate in coarse grains larger than 10 μm. The transition of deformation mechanism occurs when grain size reduces below 5 μm, which is from ⟨*a*⟩ slip and twinning to a combination of ⟨*a*⟩ slip and ⟨*c*+*a*⟩ slip, contributing to the plastic deformation and improving the ductility for the investigated Mg alloy.

3.2 Mechanical behaviors

The mechanical properties and comparisons with existing research are shown in Fig. 8. The hardness of the Mg alloys is rapidly increased with increasing aging time and reaches the peak hardness at around 1 h. After that, the hardness almost keeps unchanged with the aging time increasing. Engineering tensile stress−strain curves of T_{ex}, $T_{0.33}$, T_1, and T_8 are exhibited in Fig. 8(b), where both strength and strain of T_1 are increased compared with that of T_{ex}. The tensile yield stress (TYS), ultimate tensile stress (UTS), and tension fracture elongation (ε_{TF}) of T_1 are 314 MPa, 320 MPa, and 19%, respectively (Table 2). As shown in Figs. 8(c) and (d), the mechanical properties of the peak-aged Mg alloy are extraordinary compared with RE-free Mg alloys and even comparable to those of RE-containing Mg alloys. Notably, these properties are achieved by the conventional extrusion with low alloying content (Fig. 8(c)). Table 2 shows the summary of the mechanical properties of the investigated alloys based on Fig. 8(b).

The yield stress is usually related to grain size by the equation $\sigma_y=\sigma_0+kd^{-1/2}$, where σ_0 is friction stress, and d is average grain size. The critical grain size (5 μm) was found both in Ti alloy [34] and Mg alloy [18,35], below which twinning was eliminated, ⟨*c*+*a*⟩ and ⟨*a*⟩ slips dominate the deformation, above which twinning and ⟨*a*⟩ slip dominate [36]. The critical grain sizes for Mg−3Gd and pure Mg are

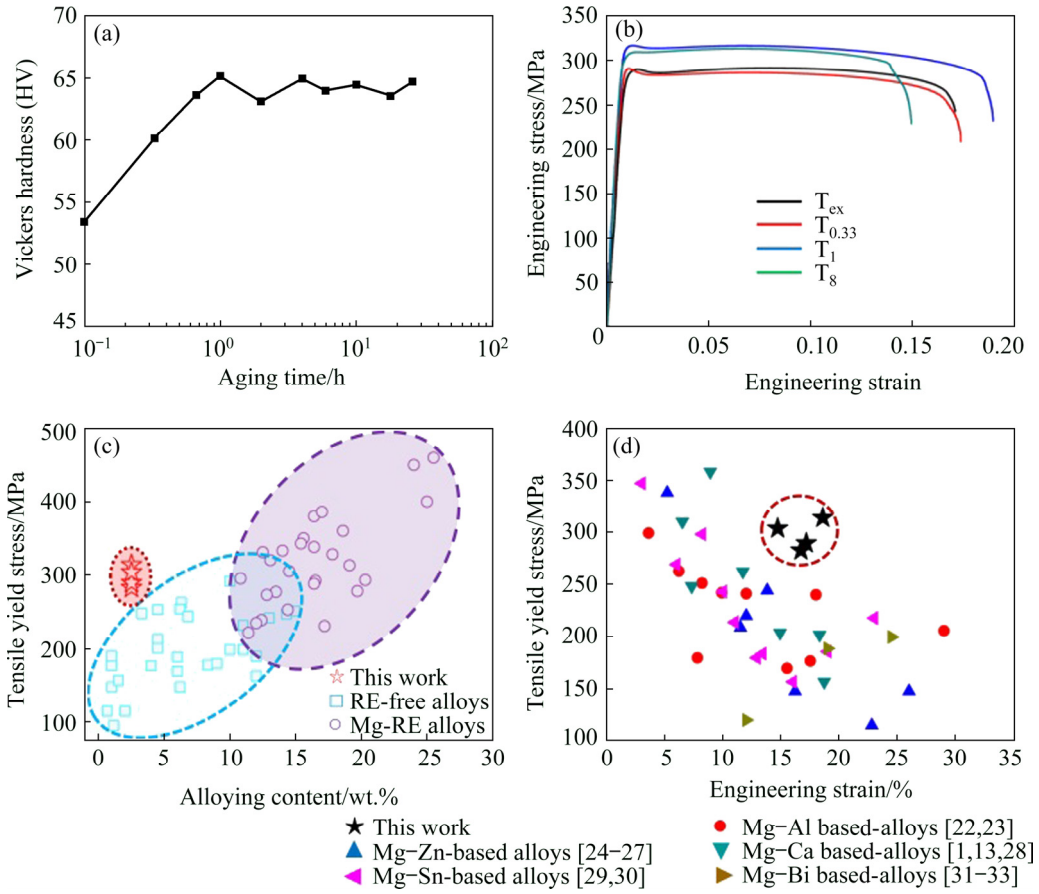

Fig. 8 Mechanical properties of alloy exhibited by aging hardening curve (a), engineering stress−strain curves (b), alloying content vs TYS (c), and strain vs TYS at room temperature with Mg−Al-based alloys [22,23], Mg−Zn-based alloys [24−27], Mg−Ca-based alloys [1,13,28], Mg−Sn-based alloys [29,30], and Mg−Bi-based alloys [31−33] (d)

Table 2 Summary of mechanical properties of investigated Mg alloys with various aging time of 20 min, 1 h and 8 h

Aging treatment	TYS/MPa	UTS/MPa	ε_{TF}/%
T_{ex}	283±1	291±1	16.7±0.1
$T_{0.33}$	289±2	293±2	17.2±0.3
T_1	314±5	320±3	19.0±0.5
T_8	304±3	313±1	14.9±0.3

~5 and 2.7 μm [10], which are significantly larger than the average grain size (1.8, 1.7 μm in T_{ex} and T_1 samples respectively) of the investigated alloy. Therefore, the deformation of the investigated Mg alloy is expected to be dominated by nonbasal ⟨*a*⟩ slips and ⟨*c*+*a*⟩ slips. After the extrusion process, the basal plane orientation of most grains is approximately parallel to ED, which is a hard orientation for basal ⟨*a*⟩ slip (i.e., low SF of basal slip). Thus, high stress is needed to operate the basal slip, following the equation of $\sigma_s=\tau_k/(\cos\varphi\cos\lambda)$. On the other hand, the weak fiber texture is in a soft orientation for nonbasal ⟨*a*⟩ and ⟨*c*+*a*⟩ slips, which is favorable to the activation of nonbasal slips [37].

Moreover, a yield point phenomenon can be observed in all aging-treated samples (Fig. 8(b)), originating from a lack of mobile dislocations in the recrystallized refined grains [10]. The extra stress is needed to operate the plastic deformation and provide an additional strengthening mechanism [18,38]. It is confirmed that there is fine Al_8Mn_5 in the extruded sample, and the GP zone is composed of Al−Ca in the aging-treated samples, which are consistent with previous research [39,40]. The existence of precipitates will impede the gliding of dislocations and strengthen the alloys following the Orowan relationship [41]. After peak-aging treatment, there is a noticeable increment of 31 and 29 MPa in TYS and UTS, respectively. Also, the ε_{TF} of the peak-aged specimen is increased by 2.3%, which is consistent with the previous study [42]. After aging, the improved ductility is attributed to the positive impacts of the GP zone on the strain-rate sensitivity avoiding the harmful effects of conventional strengthening strategies.

4 Conclusions

(1) The as-extruded sample is completely dynamically recrystallized with an average grain size of 1.8 μm. The grains are uniformly distributed, accompanied by a strong texture, which is almost unchanged after aging.

(2) The peak-aged hardness of HV 65 could be obtained after aging at 473 K for 1 h, which is HV 10 higher than that of the as-extruded sample. Furthermore, EDS results confirm that the fine precipitates are composed of Al−Mn, Al−Ca, and Al−Ca phases, which increases significantly after peak aging treatment.

(3) Fine grains can restrict the activation of twinning and promote the nonbasal slips and strong basal texture to orient towards a hard orientation for basal ⟨*a*⟩ slips, and the formation of fine precipitates is responsible for the excellent mechanical properties.

Acknowledgments

The authors are grateful for the financial supports from the Fundamental Research Funds for the Central Universities, China (Nos. 2019CDCGCL316, 2020CDJDPT001), and Chongqing Research Program of Basic Research and Frontier Technology, China (No. cstc2019jcjy-msxmX0539),

References

[1] MENG S J, YU H, FAN S D, LI Q Z, PARK S H, SUH J S, KIM Y M, NAN X L, BIAN M Z, YIN F X, ZHAO W M, YOU B S, SHIN K S. Recent progress and development in extrusion of rare earth free Mg alloys: A review [J]. Acta Metallurgica Sinica (English Letters), 2019, 32(2): 145−168.

[2] CHENG Y F, DU W B, LIU K, FU J J, WANG Z H, LI S B, FU J L. Mechanical properties and corrosion behaviors of Mg−4Zn−0.2Mn−0.2Ca alloy after long term in vitro degradation [J]. Transactions of Nonferrous Metals Society of China, 2020, 30(2): 363−372.

[3] BIAN M Z, SASAKI T T, SUH B C, NAKATA T, KAMADO S, HONO K. A heat-treatable Mg−Al−Ca−Mn−Zn sheet alloy with good room temperature formability [J]. Scripta Materialia, 2017, 138: 151−155.

[4] CHEN X, ZHANG D F, ZHAO Y, FENG J K, JIANG B, PAN F S. Microstructure modification and precipitation strengthening for Mg−6Zn−1Mn−4Sn−0.5Ca through extrusion and aging treatment [J]. Transactions of Nonferrous Metals Society of China, 2020, 30(10): 2650−2657.

[5] LIN Xiao-ping, KUO Yang, WANG Lin, YE Jie, ZHANG Chong, WANG Li, GUO Kun-yu. Refinement and strengthening mechanism of Mg−Zn−Cu−Zr−Ca alloy solidified under extremely high pressure [J]. Transactions of Nonferrous Metals Society of China, 2021, 31(6):

1587−1598.

[6] WU Z X, AHMAD R, YIN B L, SANDLÖBES S, CURTIN W A. Mechanistic origin and prediction of enhanced ductility in magnesium alloys [J]. Science, 2018, 359(6374): 447−452.

[7] LIU B Y, LIU F, YANG N, ZHAI X B, ZHANG L, YANG Y, LI B, LI J, MA E, NIE J F, SHAN Z W. Large plasticity in magnesium mediated by pyramidal dislocations [J]. Science, 2019, 365(6448): 73−75.

[8] ZHAO D X, MA X L, PICAK S, KARAMAN I, XIE K. Activation and suppression of 〈*c*+*a*〉 dislocations in a textured Mg−3Al−1Zn alloy [J]. Scripta Materialia, 2020, 179: 49−54.

[9] ZHENG R X, DU J P, GAO S, SOMEKAWA H, OGATA S, TSUJI N. Transition of dominant deformation mode in bulk polycrystalline pure Mg by ultra-grain refinement down to sub-micrometer [J]. Acta Materialia, 2020, 198: 35−46.

[10] LUO X, FENG Z Q, YU T B, LUO J Q, HUANG T L, WU G L, HANSEN N, HUANG X X. Transitions in mechanical behavior and in deformation mechanisms enhance the strength and ductility of Mg−3Gd [J]. Acta Materialia, 2020, 183: 398−407.

[11] HU F P, ZHAO S J, GU G L, MA Z D, WEI G B, YANG Y, PENG X D, XIE W D. Strong and ductile Mg−0.4Al alloy with minor Mn addition achieved by conventional extrusion [J]. Materials Science and Engineering A, 2020, 795: 139926.

[12] PENG P, HE X, SHE J, TANG A T, RASHAD M, ZHOU S B, ZHANG G, MI X X, PAN F S. Novel low-cost magnesium alloys with high yield strength and plasticity [J]. Materials Science and Engineering A, 2019, 766: 138332.

[13] PAN H C, QIN G W, HUANG Y M, REN Y P, SHA X C, HAN X D, LIU Z Q, LI C F, WU X L, CHEN H W, HE C, CHAI L J, WANG Y Z, NIE J F. Development of low-alloyed and rare-earth-free magnesium alloys having ultra-high strength [J]. Acta Materialia, 2018, 149: 350−363.

[14] TRANG T T T, ZHANG J H, KIM J H, ZARGARAN A, HWANG J H, SUH B C, KIM N J. Designing a magnesium alloy with high strength and high formability [J]. Nature Communications, 2018, 9(1): 2522.

[15] SHE J, PAN F S, GUO W, TANG A T, GAO Z Y, LUO S Q, SONG K, YU Z W, RASHAD M. Effect of high Mn content on development of ultra-fine grain extruded magnesium alloy [J]. Materials & Design, 2016, 90: 7−12.

[16] XIAO Ran, LIU Wen-cai, WU Guo-hua, ZHANG Liang, LIU Bao-liang, DING Wen-jiang. Effect of Ca content and rheo-squeeze casting parameters on microstructure and mechanical properties of AZ91−1Ce−*x*Ca alloys [J]. Transactions of Nonferrous Metals Society of China, 2021, 31: 1572−1586.

[17] NIE K B, ZHU Z H, MUNROE P, DENG K K, HAN J G. The effect of Zn/Ca ratio on the microstructure, texture and mechanical properties of dilute Mg−Zn−Ca−Mn alloys that exhibit superior strength [J]. Journal of Materials Science, 2020, 55(8): 3588−3604.

[18] LUO X, FENG Z Q, YU T B, LUO J Q, HUANG T L, WU G L, HANSEN N, HUANG X X. Transitions in mechanical behavior and in deformation mechanisms enhance the strength and ductility of Mg−3Gd [J]. Acta Materialia, 2020, 183: 398−407.

[19] KWAK T Y, LIM H K, KIM W J. The effect of 0.5 wt.% Ca addition on the hot compressive characteristics and processing maps of the cast and extruded Mg−3Al−1Zn alloys [J]. Journal of Alloys and Compounds, 2016, 658: 157−169.

[20] HUANG H, LIU H, WANG C, SUN J P, BAI J, XUE F, JIANG J H, MA A B. Potential of multi-pass ECAP on improving the mechanical properties of a high-calcium-content Mg−Al−Ca−Mn alloy [J]. Journal of Magnesium and Alloys, 2019, 7(4): 617−627.

[21] HUANG Q Y, LIU Y, TONG M, PAN H C, YANG C L, LUO T J, YANG Y S. Enhancing tensile strength of Mg−Al−Ca wrought alloys by increasing Ca concentration [J]. Vacuum, 2020, 177: 109356.

[22] PARIZI M T, EBRAHIMI G R, EZATPOUR H R. Effect of graphene nanoplatelets content on the microstructural and mechanical properties of AZ80 magnesium alloy [J]. Materials Science and Engineering A, 2019, 742: 373−389.

[23] NAKATA T, XU C, AJIMA R, SHIMIZU K, HANAKI S, SASAKI T T, MA L, HONO K, KAMADO S. Strong and ductile age-hardening Mg−Al−Ca−Mn alloy that can be extruded as fast as aluminum alloys [J]. Acta Materialia, 2017, 130: 261−270.

[24] NAKATA T, XU C, KAMADO S. Improving tensile properties of a room-temperature formable and heat-treatable Mg−6Zn−0.2Ca (wt.%) alloy sheet via micro-alloying of Al and Mn [J]. Materials Science and Engineering A, 2020, 772: 138690.

[25] LU X, ZHAO G Q, ZHOU J X, ZHANG C S, CHEN L, TANG S Q. Microstructure and mechanical properties of Mg−3.0Zn−1.0Sn−0.3Mn−0.3Ca alloy extruded at different temperatures [J]. Journal of Alloys and Compounds, 2018, 732: 257−269.

[26] DING H L, SHI X B, WANG Y Q, CHENG G P, KAMADO S. Texture weakening and ductility variation of Mg−2Zn alloy with CA or RE addition [J]. Materials Science and Engineering A, 2015, 645: 196−204.

[27] BHATTACHARJEE T, MENDIS C L, SASAKI T T, OHKUBO T, HONO K. Effect of Zr addition on the precipitation in Mg−Zn-based alloy [J]. Scripta Materialia, 2012, 67(12): 967−970.

[28] HENDERSON H B, RAMASWAMY V, WILSON-HEID A E, KESLER M S, ALLEN J B, MANUEL M V. Mechanical and degradation property improvement in a biocompatible Mg−Ca−Sr alloy by thermomechanical processing [J]. Journal of the Mechanical Behavior of Biomedical Materials, 2018, 80: 285−292.

[29] SASAKI T T, ELSAYED F R, NAKATA T, OHKUBO T, KAMADO S, HONO K. Strong and ductile heat-treatable Mg−Sn−Zn−Al wrought alloys [J]. Acta Materialia, 2015, 99: 176−186.

[30] PAN H C, QIN G W, XU M, FU H, REN Y P, PAN F S, GAO Z Y, ZHAO C Y, YANG Q S, SHE J, SONG B. Enhancing mechanical properties of Mg−Sn alloys by combining addition of Ca and Zn [J]. Materials & Design, 2015, 83: 736−744.

[31] MENG S J, YU H, LI L C, QIN J N, WOO S K, GO Y, KIM Y M, PARK S H, ZHAO W M, YIN F X, YOU B S, SHIN K

S. Effects of Ca addition on the microstructures and mechanical properties of as-extruded Mg−Bi alloys [J]. Journal of Alloys and Compounds, 2020, 834: 155216.

[32] MENG S J, YU H, ZHANG H X, CUI H W, WANG Z F, ZHAO W M. Microstructure and mechanical properties of extruded pure Mg with Bi addition [J]. Acta Metallurgica Sinica, 2016, 52(7): 811−820. (in Chinese)

[33] REMENNIK S, BARTSCH I, WILLBOLD E, WITTE F, SHECHTMAN D. New, fast corroding high ductility Mg−Bi−Ca and Mg−Bi−Si alloys with no clinically observable gas formation in bone implants [J]. Materials Science and Engineering B, 2011, 176(20): 1653−1659.

[34] YU Q, SHAN Z W, LI J, HUANG X, XIAO L, SUN J, MA E. Strong crystal size effect on deformation twinning [J]. Nature, 2010, 463(7279): 335−338.

[35] FAN H D, AUBRY S, ARSENLIS A, EL-AWADY J A. Grain size effects on dislocation and twinning mediated plasticity in magnesium [J]. Scripta Materialia, 2016, 112: 50−53.

[36] LI L, WANG Y, ZHANG C C, WANG T, LV H, YU W B. Ultrafine-grained Mg−Zn−Yb−Zr alloy with simultaneously improved strength and ductility processed by axisymmetric hot extrusion [J]. Vacuum, 2020, 173: 109157.

[37] MALIK A, WANG Y, CHENG H W, NAZEER F, KHAN M A, WANG M J. Microstructural evolution of ultra-fine grained Mg−6.62Zn−0.6Zr alloy on the basis of adiabatic rise in temperature under dynamic loading [J]. Vacuum, 2019, 168: 108810.

[38] HUANG X X, HANSEN N, TSUJI N. Hardening by annealing and softening by deformation in nanostructured metals [J]. Science, 2006, 312(5771): 249−251.

[39] CIHOVA M, SCHÄUBLIN R, HAUSER L B, GERSTL S S A, SIMSON C, UGGOWITZER P J, LÖFFLER J F. Rational design of a lean magnesium-based alloy with high age-hardening response [J]. Acta Materialia, 2018, 158: 214−229.

[40] LI Z T, ZHANG X D, ZHENG M Y, QIAO X G, WU K, XU C, KAMADO S. Effect of Ca/Al ratio on microstructure and mechanical properties of Mg−Al−Ca−Mn alloys [J]. Materials Science and Engineering A, 2017, 682: 423−432.

[41] HU F P, YU T B, LIU W T, YANG Y, WEI G B, LUO X, TANG H Y, HANSEN N, HUANG X X, XIE W D. Pt−20Rh dispersion strengthened by ZrO_2−Microstructure and strength [J]. Materials Science and Engineering A, 2019, 765: 138305.

[42] BHATTACHARYYA J J, NAKATA T, KAMADO S, AGNEW S R. Origins of high strength and ductility combination in a Guinier-Preston zone containing Mg−Al−Ca−Mn alloy [J]. Scripta Materialia, 2019, 163: 121−124.

常规热挤压制备高强韧细晶 Mg−1Mn−0.5Al−0.5Ca−0.5Zn 合金

顾光林[1,2]，柯珣楠[1]，胡发平[1]，赵淑杰[1]，魏国宾[1]，杨 艳[1]，彭晓东[1]，谢卫东[1]

1. 重庆大学 材料科学与工程学院 轻合金国际联合实验室，重庆 400044；
2. 航空工业贵州安大航空锻造有限责任公司，安顺 561005

摘 要：采用常规热挤压方法制备 Mg−1Mn−0.5Al−0.5Ca−0.5Zn 合金，挤压温度为 673 K，挤压比为 25∶1，并进行 473 K 时效处理。采用扫描电镜、电子背散射衍射和透射电镜表征合金的显微组织，测试试样的温室拉伸性能。结果表明，经 473 K、1 h 峰值时效后，试样出现细小等轴晶，平均晶粒尺寸为 1.7 μm，Al−Ca 颗粒面积分数明显增多。热挤压后仍能观察到⟨*a*⟩位错和⟨*c*+*a*⟩位错。峰值时效态样品表现出高强度和良好塑性，其抗拉强度为 320 MPa，屈服强度为 314 MPa，伸长率为 19%。

关键词：Mg−Mn−Al−Ca−Zn 合金；细晶；析出相；强度；塑性

(Edited by Xiang-qun LI)